ZKG INTERNATIONAL
ISSN / eISSN 2366-1313
Publisher BAUVERLAG BV GMBH, AVENWEDDER STR 55, GUTERSLOH, GERMANY, 33311
Volume 25-Issue 1-(2025)
https://doi.org/10.63386/61885

Directed transport of two-headed Brownian particles in a periodic microchannel under an asymmetric periodic potential

Cui Deng[1*], Xuesong Wan [2], Tingting Wang[3], Tianfeng Wu[1]

[1]College of Mathematics of Sichuan University, Chengdu 610065, Sichuan, China
[2]College of Big Data and Artificial Intelligence of Chengdu Technological University, Chengdu 611730, Sichuan, China
[3] Sichuan Aerospace Electronic Equipment Research Institute, Chengdu 610100, Sichuan, China

Corresponding author: **Cui Deng**
Corresponding email: dengcui1029@163.com

Xuesong Wan Email: wxsong19@163.com
Tingting Wang Email: wangtting116@163.com
Tianfeng Wu Email: Functions2010@yeah.net

Funding

This work was supported by Talent Project Foundation of Chengdu Technological University (No.2550023)

Abstract

Building upon experimental observations of molecular motor transport phenomena, we conducted a theoretical and computational analysis of the diffusive dynamics in a system of elastically coupled particles subjected to an asymmetric periodic potential in a two-dimensional periodic microchannel, to reveal the dynamical mechanism of cooperative transport of particles with two heads. While moving in a confined structure, Brownian particles could display non-equilibrium transport anomalies. The dependence of directed current on various parameters is systematically studied. Our results indicate that the direction of motion can be reversed by modulating the coupling strength, free length, maximum width of the microchannel, and frequency of microchannel width variation. In addition, we have discussed the generalized stochastic resonance phenomenon with the variation of each parameter in the strong-coupling case. These research findings are helpful for studying complex systems such as transport through nuclear pores and cellular transport along protein filaments, and also provide a technologically viable strategy for optimizing and manipulating collective directed transport through systematic parameter engineering.

Keywords

Directed transport; Coupled Brownian particles; Periodic microchannel; Overdamped; Symmetric periodic potential

1. Introduction

In recent decades, the problem of cooperative directional transport has emerged as a pivotal research focus in Brownian particle dynamics. This cross-disciplinary challenge has garnered substantial attention from physicists, biologists, chemists, and mathematicians, yielding groundbreaking findings [1-16]. For example, Mahadevan's biological experiments demonstrated that many molecular motors (e.g., kinesin, myosin, dynein) operates as bipedal motors with synergistic activity between strongly coupled pairs [1,2]; Guérin's group discovered that collective directional transport emerges only when multiple myosin-II proteins collaborate, whereas single proteins remain inactive [4]; Liu et al. developed a theoretical framework for 2D coupled ratchet transport systems [10]; In 2025, Peng et al. systematically analyzed directional transport performance of coupled Brownian particles in rough potentials [16]. These phenomena reveal that emergent collective dynamics produce complex behaviors not observed in single-particle systems, and highlight the mechanistic necessity of studying cooperative Brownian transport.

However, in most of the investigations, the external potential is free, without thinking about the boundary. Accumulating evidence demonstrates that boundary constraints in microchannels significantly influence Brownian particle transport behaviors [17–31]. For example, Bao et al. demonstrated that the drag force influence of slip boundary conditions and gas rarefaction changes the particles' residential time [23]; Guo et al. revealed that collective motion directionality is entirely governed by channel asymmetry [27]. Notably, boundary-constrained transport studies exhibit critical practical implications across systems such as carbon nanotube dynamics [17], brain tissue microstructure [18], membrane permeability [26], and porous media transport [31]. This gives us an enlightenment for setting up the ratchet model of coupled Brownian particles in confined geometries.

Motivated by the previous research, we investigated an overdamped Brownian motion of two coupled particles with an asymmetric periodic potential in a two-dimensional periodic microchannel theoretically and numerically, to reveal the dynamical mechanism of cooperative transport of particles with two heads. We will focus on the effects of the coupling strength, maximum width of the microchannel，and frequency of microchannel width variation on the particle transport behavior with the appropriate noise periods in this paper. In addition, we have discussed the generalized stochastic resonance phenomenon with the variation of each parameter in the strong-coupling case.

2. Coupled Langevin system

2.1. System model

In this paper, we consider an overdamped Brownian motion of two coupled particles with an asymmetric periodic potential in a two-dimensional periodic microchannel. First, we introduce a coupled two-particle system based on the Frenkel-Kontorova (FK) model grounded in classical mechanics principles [32], which describes the motion dynamics of a particle chain in a potential field. The schematic diagram is shown in Fig. 1.

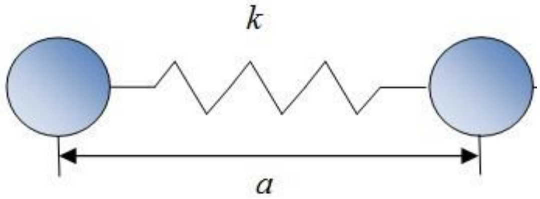

Figure 1. Schematic diagram of the model for two particles.

The equations of motion of two coupled particles can be mathematically represented by

$$\mu \ddot{x}_i = -\frac{\partial V\left(x_i\right)}{\partial x_i} - \frac{\partial U}{\partial x_i} + \xi_{x,i}\left(t\right), i = 1,2 \tag{1}$$

$$\mu \ddot{y}_i = \begin{cases} 0, \left|y_i\right| > d(t,x_i)/2 \\ -\frac{\partial U}{\partial y_i} + \xi_{y,i}\left(t\right), \left|y_i\right| \le d(t,x_i)/2 \end{cases}, i = 1,2 \tag{2}$$

where (x_i, y_i) is the position of the i-th particle, μ is the friction coefficient. When the friction coefficient μ is constant, it doesn't affect the analysis of the results. Thus, we have μ=1 in this paper. When the particle reaches the boundary of the microchannel, the energy of the particle will be fully absorbed, which satisfies the Dirichlet boundary condition. Throughout this paper, we suppose the size of the particle is negligible.

The time-dependent width $d(t,x)$ of the microchannel is governed by:

$$d(t,x) = \frac{d_0}{2}(\sin(2\pi(x - \upsilon_0 t)) + 1), \tag{3}$$

where d_0 is the maximum width of the microchannel, υ_0 is the frequency of microchannel width variation.

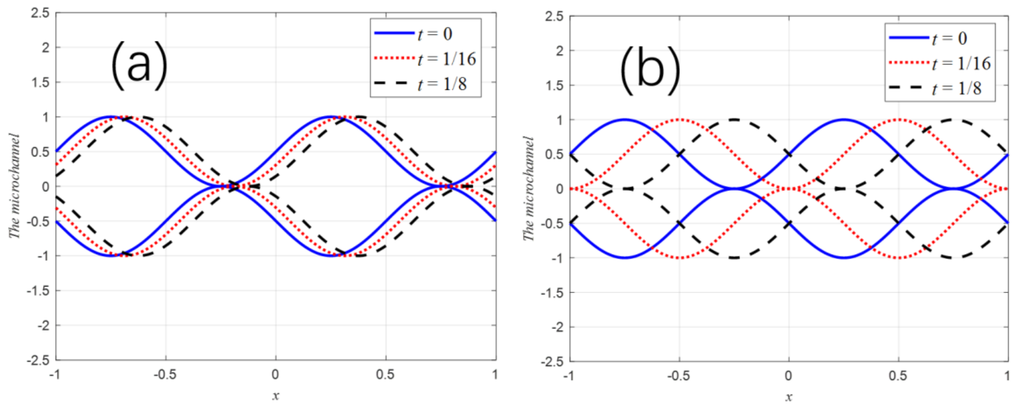

Figure 2. Microchannel schematic diagram for the case: (a) υ_0=1; (b) υ_0=2. The other parameter is set to be d_0=2.

Fig. 2 shows the microchannels at different frequency changes. It can be seen that the changes with time when υ_0=2 are faster than the case when υ_0=1. Meanwhile, when υ_0=2 and $t = \frac{1}{16}$, the microchannel states are the same as the case when υ_0=1 and $t = \frac{1}{8}$.

$V\left(x\right)$ is the asymmetric periodic potential arising from the interaction between the particles and the track of x-coordinate. The following simplified form of $V\left(x\right)$ is chosen:

$$V\left(x_i\right) = -V_0\left[\sin\left(\frac{2\pi}{L}x_i\right) + \frac{\Delta}{4}\sin\left(\frac{4\pi}{L}x_i\right)\right], \tag{4}$$

where V_0 is the potential strength, Δ is the asymmetry coefficient of $V(x)$, and L is the spatial period of $V(x)$. Throughout this paper, we set the parameters V_0=1.

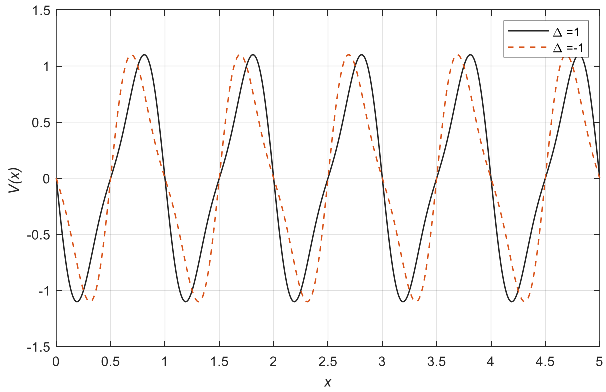

Figure 3: The asymmetric periodic potential $V(x)$ with Δ=$\{$-1,1$\}$ for the case V_0=1, $L=1$.

The interaction potential $U(\vec{P}_1,\vec{P}_2)$ between the two particles is defined by the following harmonic function:

$$U(\vec{P}_1,\vec{P}_2)=\frac{k}{2}\left(\left|\vec{P}_1-\vec{P}_2\right|-a\right)^2, \vec{P}_1=(x_1,y_1), \vec{P}_2=(x_2,y_2), \tag{5}$$

where k is the coupling strength, and a is the coupling free length.

The effect of the two reservoirs on the particles is modeled as thermal noises

$$\vec{\xi}_i(t)=(\xi_{x,i}(t),\xi_{y,i}(t)), i=1,2, \tag{6}$$

which are assumed to be independent, unbiased Gaussian white noises with

$$\langle\xi_{x,i}(t)\rangle=\langle\xi_{y,i}(t)\rangle=\langle\xi_{x,i}(t)\xi_{y,i}(t)\rangle=0, \tag{7}$$

$$\langle\xi_{x,i}(t)\xi_{x,j}(t')\rangle=\langle\xi_{y,i}(t)\xi_{y,j}(t')\rangle=2k_BT_i(t)\delta_{ij}\delta(t-t'), \quad i,j=1,2, \tag{8}$$

where k_BT is the thermal energy, and $T_1(t)$, $T_2(t)$ are the following modulated harmonically varying functions:

$$T_1(t)=T_0\left[1+A\sin\left(\frac{2\pi}{t_0}t\right)\right]^2, \tag{9}$$

$$T_2(t)=T_0\left[1+A\sin\left(\frac{2\pi}{t_0}t+\Delta\theta\right)\right]^2, \tag{10}$$

where t_0 is the pulsation period of the temperature, and $\Delta\theta$ is the phase shift between two temperature fluctuations.

In the aforementioned temperature ratchet model, the maximum temperature corresponds to the minimum binding of the potential well, and the minimum temperature corresponds to the strongest binding to the coupled particles.

According to the Eq. (9) and Eq. (10), the temperature fluctuation of both particles is synchronized with $\Delta\theta$=0, which means that the average velocity reaches the maximum value because the coupling could enhance the motion. For $\Delta\theta = \pi$, one temperature of the coupled motors reaches the maximum value when the other one is at the minimum, indicating that the coupling reduces the motion of the coupled particles in this case [32].

Throughout this paper, we set the parameters T_0=0.5 , A=0.8 and $t_0 = 1$.

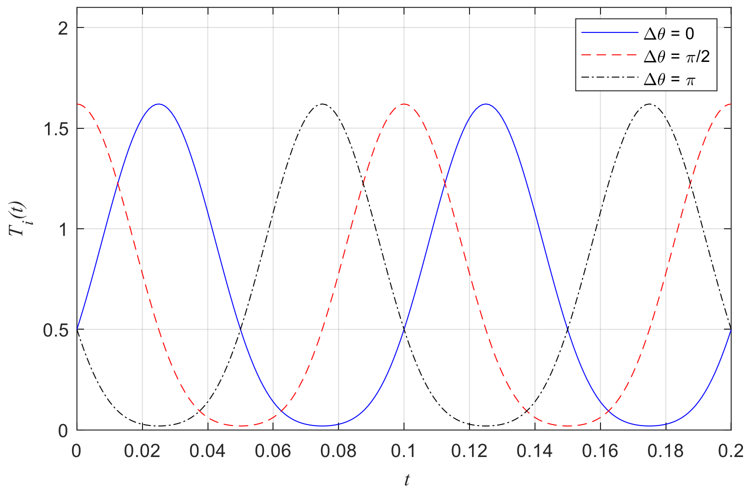

Figure 4. T_i in Eq. (9) and Eq. (10) respectively with $\Delta\theta = \{0, \pi/2, \pi\}$ as a function of parameter t for the case T_0=0.5 , A=0.8 , $t_0 = 1$.

The primary quantity of interest is the average velocity derived from both ensemble and time averaging of the instantaneous velocities. Considering that the motion of the particles in y -direction is constrained by the boundary, we mainly study that in the x -direction:

$$v = \lim_{T\to\infty} \frac{1}{2T} \sum_{i=1}^{2} \int_0^T \dot{x}_i(t) dt , \tag{10}$$

where T is the transport duration. The average velocity is a macroscopic quantity which can be measured in a real experiment.

2.2 The principle of coupled particles transport

Based on Eq. (1), it can be seen that the particle motion is subject to the combined action of potential field force ($F_1 = -\frac{\partial V(x_i)}{\partial x_i}$) , coupling force ($F_{2x} = -\frac{\partial U}{\partial x_i}$ and $F_{2y} = -\frac{\partial U}{\partial y_i}$) and thermal noise ($\xi_{x,i}$ and $\xi_{y,i}$) . The respective effects of the three forces are concisely summarized below, with detailed analysis provided in [22].

2.2.1. Potential Field Force

The influence of the external potential in the x -direction on the transport of the coupled particles is first visualized through the position diagram (see Fig.5) and the potential field force diagram (see Fig.6) of the two particles at different microchannel width.

As can be seen from Fig. 5, when the microchannel width is narrow [e.g., $d = 0.1$], the particles are restricted to the x -direction due to spatial confinement in width, so the two particles have a larger spacing in the x -direction, as shown the relative positions of particle 1 and particle 2 in Fig. 5. When the microchannel width is wide [e.g., $d = 1$], the particles can move in both the x -direction and the y -direction, so the distance between the two particles in the x-direction is relatively narrow, as shown the relative positions of particle 1 and particle 2′ in Fig. 5.

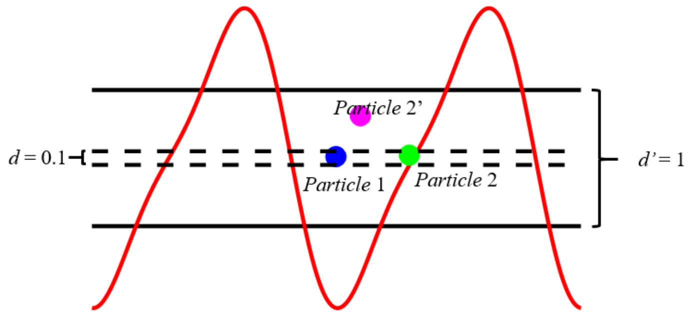

Figure 5. Schematic diagram of position of the particle

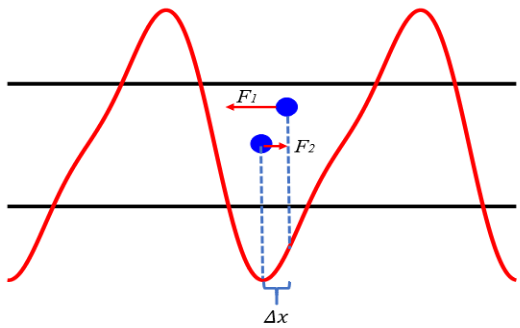

Figure 6. Schematic diagram of potential field force F of the particle

From the Eq. (1) and Eq. (2), it is found that the potential field force of the particle is only affected by the horizontal position, as shown in Fig. 6, therefore the resultant force of external potential is determined by the average horizontal interval Δx which is the mean of $|x_1 - x_2|$. Because of the rotational symmetry [33], we study the case where $\Delta x \le 0.5L$ in the following discussion.

When $\Delta x < 0.25L$, the probability that the resultant force of external potential is negative is greater than 50%. Thus, the potential field force makes particles tend to move in a negative direction. Whereas the probability that the resultant force of external potential is positive is greater than 50% when $0.25L < \Delta x < 0.5L$, and it makes particles tend to move in a positive direction.

2.2.2 Coupling Force

In the case of weak-coupling [e.g., $0.01 < k < 1$], the transport behavior of the coupled particles degrades into that of single particle. At this time, the relationship between particles is unstable, and the external potential resultant force of two particles is reflected as random action.

In the case of strong-coupling [e.g., $40 < k < 1000$], the relative relationship between particles is stable. At this time, the distance between particles is close to the free length of particles, and the resultant force of external potential is relatively stationary as well.

2.2.3 Thermal Noise

From the Eq. (9) and Eq. (10), for an infinitely large pulsation period t_0, the temperature pulsates so slowly that it can be regarded as a constant. In this case, the coupled Brownian particles are immersed in a stationary periodic potential and a white Gaussian noise with a constant intensity, where the system has a null directed current regardless of the coupling strength k. In contrast, when t_0 tends to zero, the temperature fluctuates too rapidly, and the change in the configuration of the coupled Brownian particles always lags behind the rapid temperature fluctuation. This also leads to an absence of directed motion [32].

Therefore, it is only possible to generate directed current under appropriate noise periods [e.g., $t_0 = 0.1$].

3. Simulations and analysis

3.1 The simulation method

In this paper, the stochastic Runge-Kutta method is employed to numerically solve the equations of motion and we set the transport duration to be $T = 100s$. Moreover, a total of 500 simulations were performed.

3.2 Analysis of results

3.2.1 Effect of coupling strength on the transport behavior

The coupling strength k critically influences the directed transport in the ratchet system. Fig. 7 shows three curves of the average velocity against the coupling strength k with phase shifts $\Delta\theta = \{0, \pi/2, \pi\}$.

For every curve in Fig. 7, the sign of the velocity, which corresponds to the direction of motion of the coupled particles, exhibits a non-monotonic variation with increasing coupling strength, demonstrating an initial reduction followed by a recovery. For weak coupling [e.g., $0.01 < k < 1$], the average velocity $v \approx -0.22$, which is regarded as a constant. This is because in the weak-coupling case, the motion can be considered as that of two single particles. With increasing coupling strength k [e.g., $1 < k < 40$], coupling gradually begins to inhibit transport velocity, which shows that the coupling between the two coupled particles affects the symmetry breaking of the entire system.

In addition, we find that the three transport velocity trajectories exhibit minimal variation when $k < 40$, which shows different phase shifts are not enough to affect the motion of the particles. That is also because of the single-particle behavior and the fact that the mean velocity is independent of $\Delta\theta$ for the weak-coupling case.

When the coupling is large enough [e.g., $40 < k < 1000$], the transport velocities of particles under identical coupling strength exhibit a distinct hierarchy: $v_{\Delta\theta=0} > v_{\Delta\theta=\pi/2} > v_{\Delta\theta=\pi}$. This velocity ordering can be interpreted through the lens of noise-induced transport theory. For $\Delta\theta = 0$, the noise of both particles is synchronized, which means that the average velocity reaches the maximum value because the coupling could enhance the motion. For $\Delta\theta=\pi$, one of the coupled particles is subjected to strong noise when the other one is acted to the weakest, indicating that the coupling reduces the motion of the coupled motor in this case. Therefore, transport velocity of the particles is inhibited. This also can be interpreted in terms of the formulas, Eq. (9) and Eq. (10), for the two temporally modulated temperatures.

Based on the above analysis, the following discussions will further analyze the influence of other parameters on the transport behavior in the strong-coupling case.

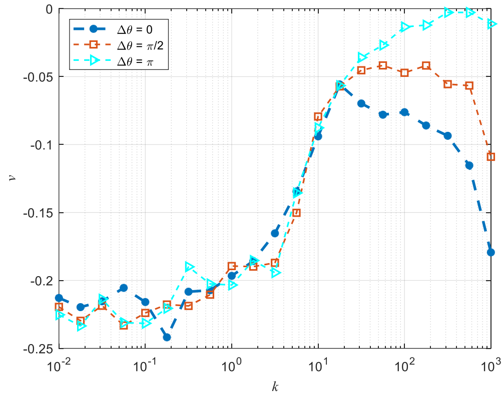

Figure 7. The velocity v respectively with $\Delta\theta=\{0,\pi/2,\pi\}$ as a function of coupling strength k. The other parameters are set to be a=0.3L, $L=1$.

3.2.2 Effect of maximum width of the microchannel on the transport behavior

As can be seen from above analysis in Section 2.2.1, the resultant force of external potential is determined by the average horizontal interval Δx. However, microchannel width d will affect Δx, as shown in Fig. 3. That is, the resultant force of external potential is directly modulated by the microchannel width, which is determined by the maximum width and the variation frequency. Therefore, in this and the next sections, we will systematically investigate the effects of the maximum width and the variation frequency of the microchannel width on the particle transport in the strong-coupling case [e.g., k=1000].

In Fig. 8 and Fig. 9, we respectively give the average velocity versus the microchannel maximum width d_0 with phase shifts $\Delta\theta=\{0,\pi/2,\pi\}$ for the case a=0.3L and $a=0.1L$ by Monte Carlo method, where two curves correspond to different microchannel width variation frequency υ_0.

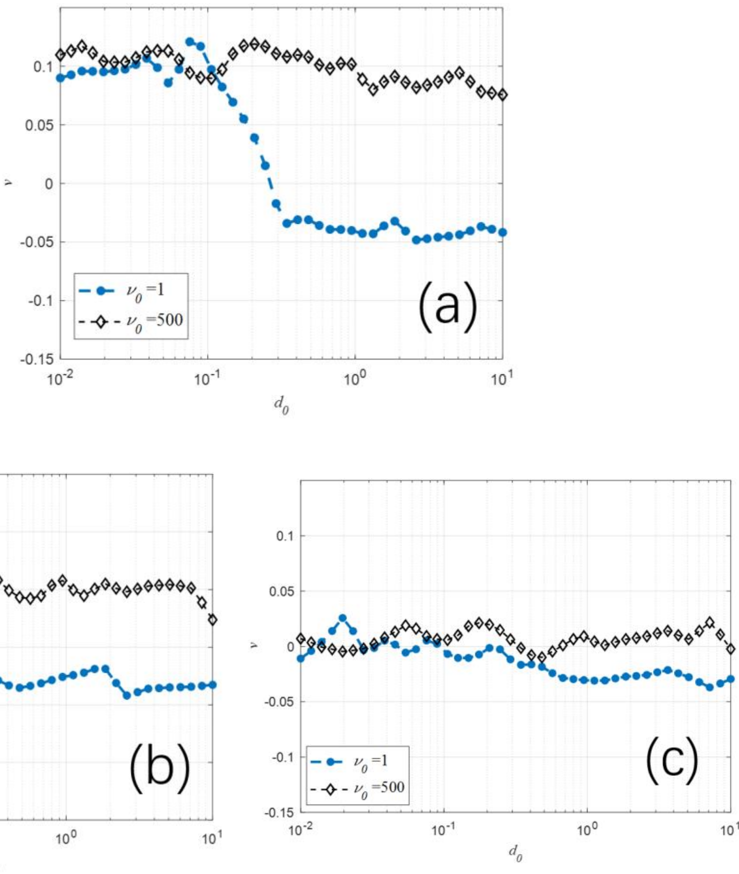

Figure 8. The velocity v respectively with $\upsilon_0 = \{1,500\}$ as a function of the maximum width of microchannel d_0 for the case: (a) $\Delta\theta=0$; (b) $\Delta\theta=\pi/2$; (c) $\Delta\theta=\pi$. The other parameters are set to be $a=0.3L$, $L=1$.

From Fig. 8, for small values of d_0 [e.g., $d_0<0.2$], it is obvious to find that the particles tend to the positive transport. Because when the microchannel width is narrow, the horizontal distance of two particles is longer on account of the limit of microchannel boundary. However, when the width of the microchannel changes relatively slowly at $\upsilon_0=1$, the particles can remain free from the limitation of the microchannel width for a long time as the width is large enough so that the horizontal distance begins to decline, and then the particles gradually produce negative transport. When the frequency of the microchannel width variation has been significantly increased at $\upsilon_0=500$, The particles are subjected to frequent confinement due to the narrowing microchannel, leading to almost no change in horizontal distance. Therefore, the particles exhibit insensitivity to changes in the microchannel maximum width and the particles produce positive transport in this case. This is consistent with the analysis in Section 2.2.1.

In addition, as the maximum width increases continuously with $\upsilon_0=500$, transport velocity of the particles is gradually inhibited, the effect of the potential field force weakens, while asynchronous noise begins to suppress particle motion, ultimately leading to a reduction in transport velocity, which is consistent with the above analysis results in Section 2.2.3. Through the aforementioned analysis, it can be observed that the frequency of the microchannel width variation has a significant impact on particle transport behavior. This will be analyzed in detail in Section 3.3 of the following content.

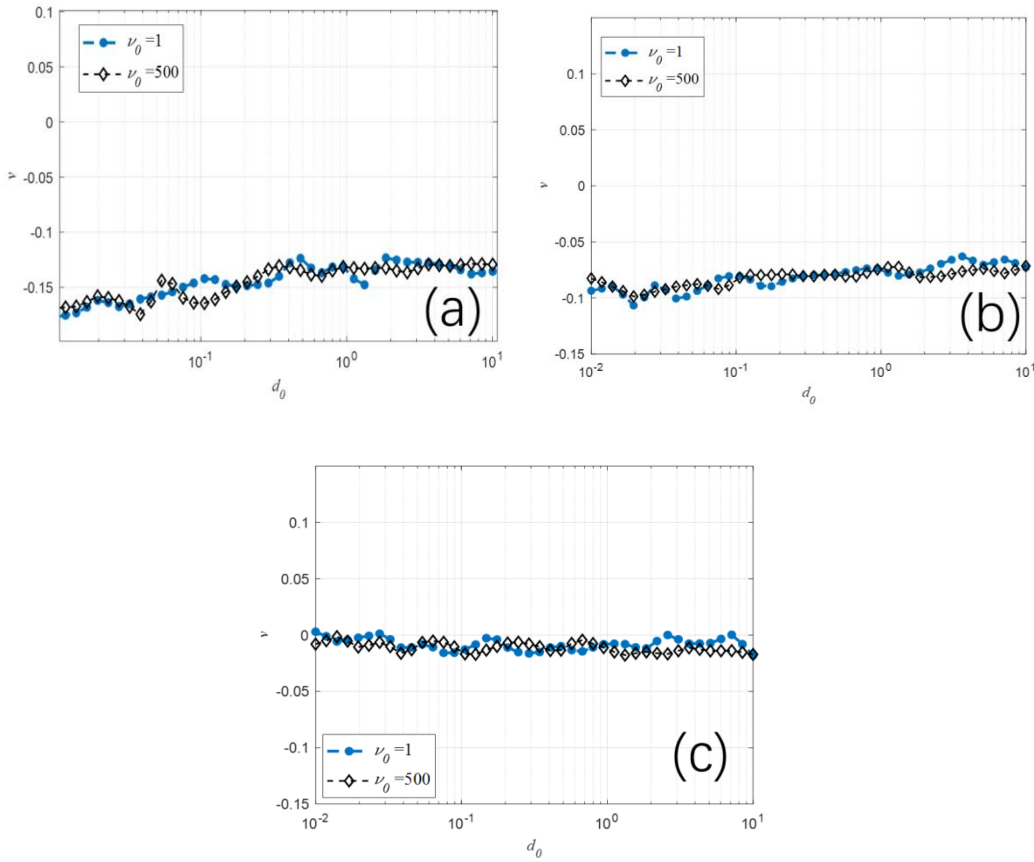

Figure 9. The velocity v respectively with $\upsilon_0 = \{1,500\}$ as a function of the maximum width of microchannel d_0 for the case: (a) θ=0 ; (b) $\Delta\theta$=$\pi/2$; (c) $\Delta\theta$=π . The other parameters are set to be $a = 0.1L$, $L = 1$.

As can be seen from Fig. 9, the curves have almost no change with increasing the maximum width. This is because when the free length is enough short, the transport between the two particles is less constrained by the microchannel width variation.

3.2.3 Effect of frequency of the microchannel width variation on the transport behavior

In Fig. 10 and Fig. 11, we respectively give the average velocity versus the frequency of the microchannel width variation υ_0 with phase shifts $\Delta\theta = \{0, \pi/2, \pi\}$ for the case a=0.3L and $a = 0.1L$ by Monte Carlo method, where four curves correspond to different microchannel maximum width d_0.

By observing the curves in Figure 10 when d_0=0.01 and d_0=0.1 , we find that the fluctuations of the two curves are slight. This is because the width of the microchannel is relatively narrow so that the variation frequency has little effect on the horizontal distance of particles, resulting in positive transport and indicating that the variation frequency has almost no influence on the transport velocity under these confinement conditions.

However, when the width of the microchannel is relatively wide [e.g. d_0=0.7] and the frequency of the width variation is relatively low, the particles can remain free from the limitation of the microchannel width for a long time. Thus, the width of the microchannel has almost no effect on the transport velocity of the particles in this case. As the frequency of microchannel width variation increases, the limitation imposed by the microchannel width begins to become prominent. The particles start to be influenced by the microchannel and exhibit positive transport behavior. As the frequency of microchannel width variation continues to increase, the positive transport velocity is gradually suppressed.

As can be seen from Fig. 11, the curves have almost no change with the variation frequency increasing. This is also because when the free length is short enough, the transport between the two particles is less constrained by the microchannel width, which is similar to the situation shown in Fig. 9. These simulation results match perfectly with the above theoretical analysis.

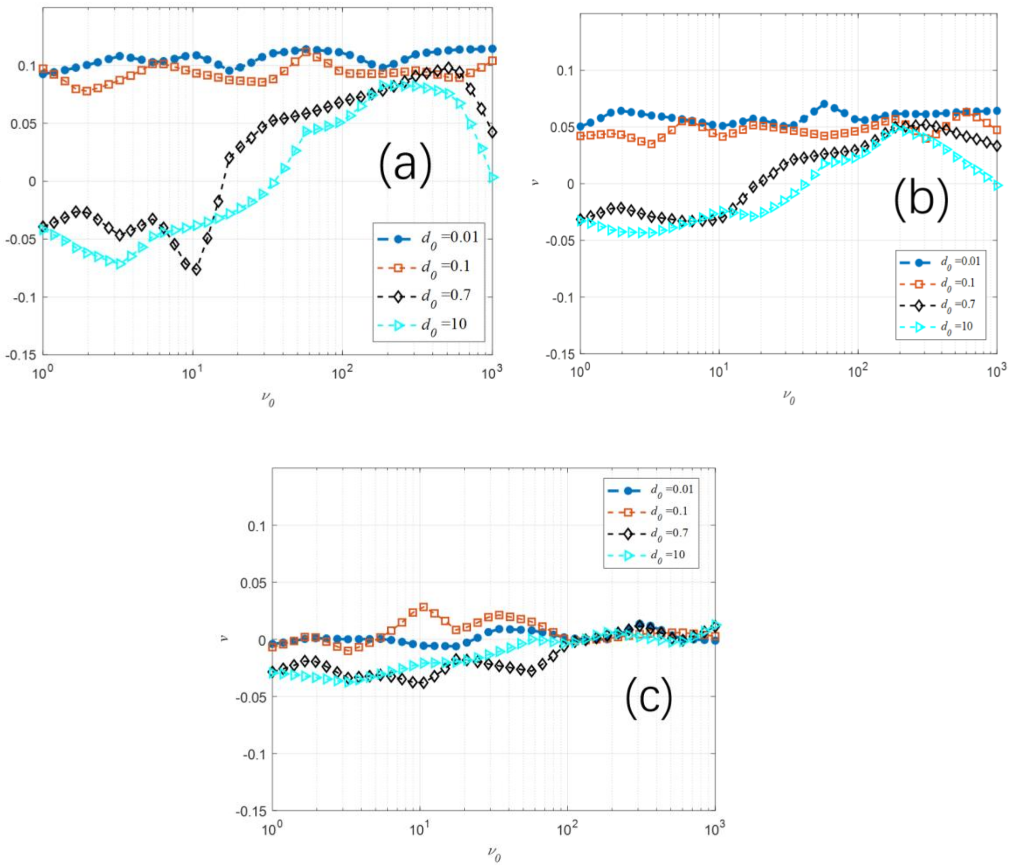

Figure10. The velocity v respectively with $d_0 = \{0.01, 0.1, 0.7, 10\}$ as a function of the frequency of microchannel variation υ_0 for the case: (a) $\Delta\theta$=0 ; (b) $\Delta\theta=\pi/2$; (c) $\Delta\theta=\pi$. The other parameters are set to be a=0.3L , $L=1$.

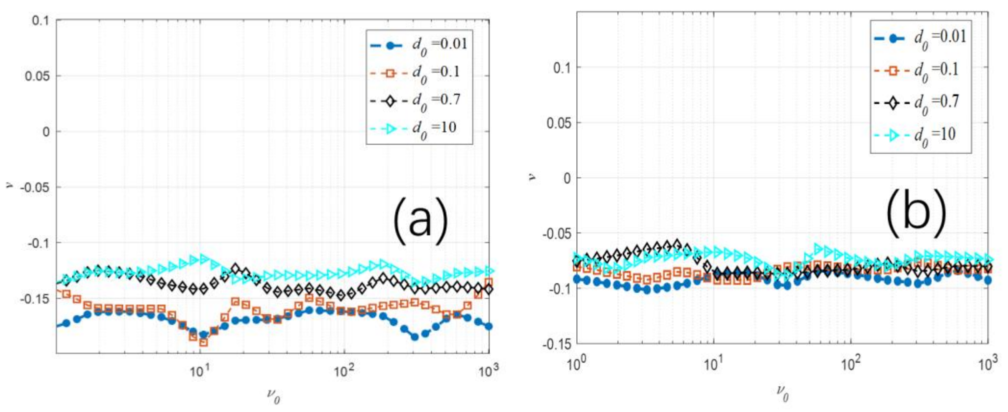

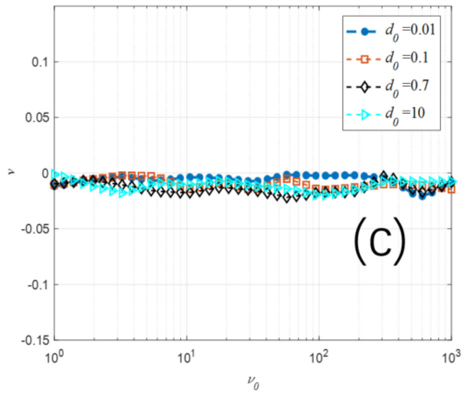

Figure 11. The velocity v respectively with $d_0 = \{0.01, 0.1, 0.7, 10\}$ as a **function** of the frequency of microchannel variation υ_0 for the case: (a) $\Delta\theta=0$; (b) $\Delta\theta=\pi/2$; (c) $\theta=\pi$. The other parameters are set to be $a = 0.1L$, $L = 1$.

4. Discussion of generalized stochastic resonance

According to the preceding analysis, the particles in periodically varying boundary systems will exhibit richer transport behavior when the free length between particles $a=0.3L$ and the noise among particles is synchronized. Fig. 12, Fig. 14 and Fig. 16 respectively demonstrate the generalized stochastic resonance phenomenon under strong coupling and synchronized noise conditions. For small maximum microchannel widths, negative stochastic resonance occurs as the variation frequency increases, while positive stochastic resonance is observed for large widths, specific as follows.

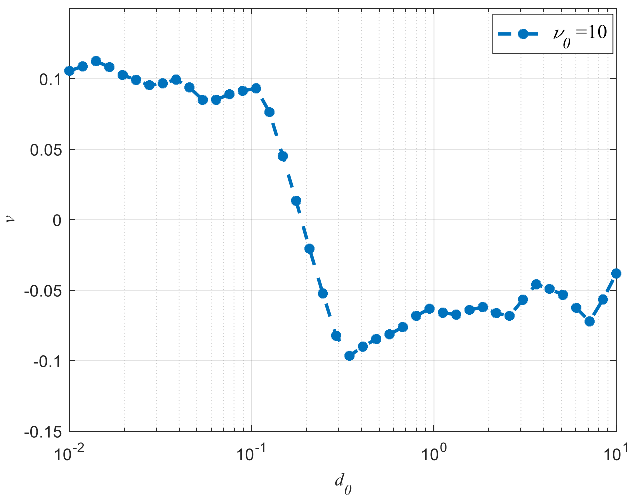

Figure 12. The velocity v respectively with $\upsilon_0 = 10$ as a function of the **maximum** width of microchannel d_0 . The other parameters are set to be $\Delta\theta=0$, $a=0.3L$, $L = 1$.

Fig. 12 curves the transport velocity varying with the maximum width of the microchannel. It can be seen that as the maximum width increases continuously, the transport velocity exhibits an initial positive-to-negative transition, reaching a maximum negative transport velocity. Further increasing the maximum width begins to suppress the negative transport velocity, resulting in a generalized negative stochastic resonance phenomenon.

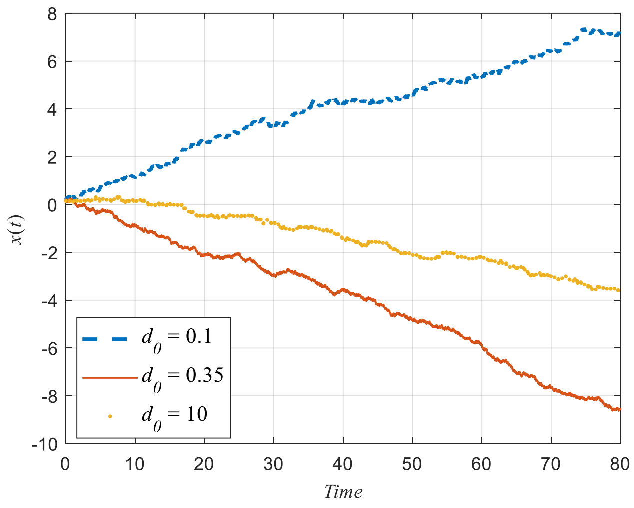

Figure 13. The trajectory of particle transport **respectively** with $d_0 \in \{0.1, 0.35, 10\}$, where $\upsilon_0 = 10$. The other parameters are set to be $\Delta\theta = 0$, $a = 0.3L$, $L = 1$.

Fig. 14 plots the transport velocity versus the frequency of microchannel width variation with $d_0 \in \{0.25, 0.34, 0.48, 1.32\}$. It can be seen that when the microchannel maximum width is relatively small, as the frequency of the microchannel width variation increases continuously, the transport velocity first reaches the maximum value in a negative direction. Further increasing the maximum width begins to begins to suppress the negative transport velocity, generating generalized negative stochastic resonance behavior, and ultimately causing the particles to exhibit positive transport.

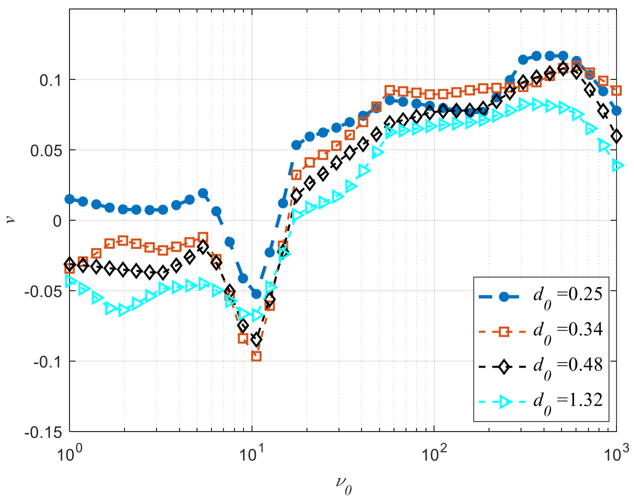

Figure 14. The velocity v respectively with $d_0 \in \{0.25, 0.34, 0.48, 1.32\}$ as a **function** of the frequency of microchannel variation υ_0. The other parameters are set to be $\Delta\theta = 0$, $a = 0.3L$, $L = 1$.

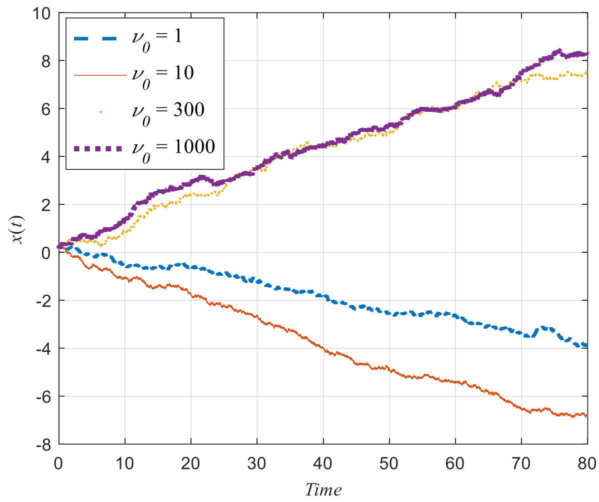

Figure 15. The trajectory of particle transport respectively with $\upsilon_0 \in \{1,10,300,1000\}$,**where** $d_0 = 0.25$. The other parameters are set to be $\Delta\theta=0$, $a=0.3L$, $L=1$.

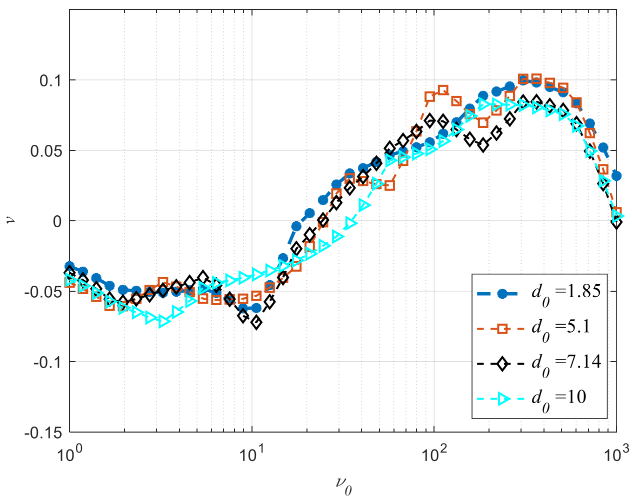

Figure 16. The velocity v respectively with $d_0 \in \{1.85,5.1,7.14,10\}$ as a **function** of the frequency of microchannel variation υ_0 . The other parameters are set to be $\Delta\theta=0$, $a=0.3L$, $L=1$ ..

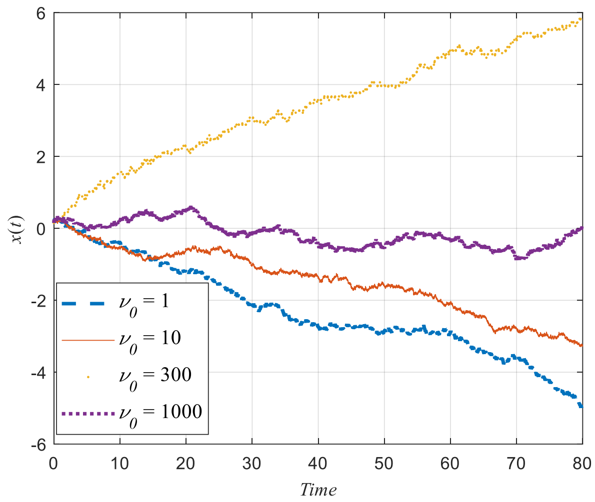

Figure 17. The trajectory of particle transport respectively with $\upsilon_0 \in \{1,10,300,1000\}$,where $d_0 = 10$. The other parameters are set to be $\Delta\theta=0$, $a=0.3L$, $L=1$.

Fig. 16 curves the transport velocity varying with the frequency of microchannel variation with $d_0 \in \{1.85,5.1,7.14,10\}$. It can be seen that when the microchannel maximum width is relatively large, as the maximum width increases continuously, the transport velocity exhibits an initial negative-to-positive transition, reaching a maximum positive transport velocity. Further increasing the frequency variation begins to suppress the negative transport velocity, resulting in a generalized positive stochastic resonance phenomenon.

In Fig. 13, Fig. 15 and Fig. 17, some trajectories of particle transport are respectively given based on the above-mentioned resonance phenomenon.

5. Conclusions

Above all, we have investigated the transport properties of coupled Brownian particles confined to a periodic microchannel in an asymmetric periodic potential theoretically and numerically, to reveal the dynamical mechanism of cooperative transport of particles with two heads. In this paper, the relations between directed transport on various parameters (coupling strength, free length, maximum width of the microchannel，and frequency of microchannel variation width) on the transport behavior is analyzed sequentially, and the computer simulation results about the above parameters were consistent with the theoretical analysis. Moreover, when the maximum width of the microchannel is relatively small, the generalized negative stochastic resonance behavior is observed as the variation frequency increases, whereas generalized positive stochastic resonance behavior occurs when the maximum width is relatively large. These research findings are helpful for studying complex systems such as transport through nuclear pores and cellular transport along protein filaments, and also provide a technologically viable strategy for optimizing and manipulating collective directed transport through systematic parameter engineering.

References

1. Mahadevan, L.; Matsudaira, P. Motility powered by supramolecular springs and ratchets. *Science* 2000, *288*, 95-99.
2. Badoual, M.; Julicher, F.; Prost, J. Bidirectional cooperative motion of molecular motors. *Proc. Natl. Acad. Sci. U.S.A.* 2002, *99*, 6696-6701.

3. Omabegho, T.T.; Sha, R.; Seeman N. C. A Bipedal DNA Brownian motor with coordinated legs. *Science* 2009, *324*, *6*7-71.
4. Guerin, T.; Prost, J.; Martin, P. Coordination and collective properties of molecular motors: theory. *Current Opinion in Cell Biology* 2010, *22*, 14-20.
5. Zhang, X.; Cao, J.H.; Ai, B.Q.; Gao, T.F.; Zheng, Z.G. Investigation on the directional transportation of coupled Brownian motors with asymmetric friction. *Acta Phys. Sin.* 2020, *69*,100503.
6. Wu, W.X.; Zheng, Z.G.; Song, Y.L.; Han, Y.R.; Sun, Z.C.; Li C.P. Directed transport of coupled Brownian motors in a two-dimensional traveling-wave potential. *Chin. Phys. B* 2020, 9, 090503.
7. Wang, Y.; Zeng, C.H.; Ai, B.Q. Anomalous transport and diffusion of coupled Brownian particles with periodic driving forces. *European physical journal plus* 2021, *136*, 1071.
8. Spiechowicz, J.; Łuczka, J. Energy of a free Brownian particle coupled to thermal vacuum. *Scientific reports* 2021,*11*,4088.
9. Ahuja, V.R.; Gucht, J.V.D.; Briels, W. Large scale hydrodynamically coupled Brownian dynamics simulations of polymer solutions flowing through porous media. *Polymers* 2022, 14, 1422.
10. Liu, Y.Y.; Sun, J.M.; Fan, L.M.; Gao, T. F. Zheng, Z.G. Directional transport of two-dimensional coupled Brownian particles subjected to nonconserved forces. *Acta Phys. Sin.* 2023, *72*, 040501.
11. Colangeli, M.; Duong, M.H.; Muntean, A. Model reduction of Brownian oscillators: quantification of errors and long-time behavior. *Journal of Physics A: Mathematical and Theoretical* 2023, 56, 345003.
12. Archanal, G.R.; Barik, D. Multiple current reversals in driven inertial coupled Brownian particles under rough symmetric periodic potential. *Physica A* 2024, *650*, 129992
13. Zhang, P.J.; Zhang, J.Q.; Wang, P.; Huo, J.; Wang, X.M. Directed transport of two-coupled particles under the coordination of the coupling and an asymmetric potential *Chaos, Solitons and Fractals* 2024 182, 114830.
14. Archana, G.R.; Barik, D. Multiple current reversals in driven inertial coupled Brownian particles under rough symmetric periodic potential. *Physica A* 2024, 650, 129992.
15. Azizi, E.; Mostufa, S.; Rezaei, B.; Xin, S.M.; Sun, J.J.; Shi, Z.Q.; Gómez-Pastora, J.; Wu, K. Applying stochastic Langevin function with coupled Brownian–Néel relaxations to study the dynamic magnetizations of nanoparticle tracers in magnetic particle imaging *J. Phys. D: Appl. Phys.* 2025, 58, 135002.
16. Peng, J; Zhao, G.K.; Wang, P.; Huo, J.; Wang, X.M. Directed transport of two-coupled Brownian particles in a rough potential. *Chaos, solitons and fractals* 2025, *194*, 116204
17. Hummer, G.; Rasaiah, J.C.; Noworyta, J. Water Conduction through the Hydrophobic Channel of a Carbon Nanotube. *Nature* 2001, *414*, 188-190.
18. Santamaria, F.; Wils, S.; Schutter, E.D.; Augustine, G.J. Anomalous diffusion in Purkinje cell dendrites caused by spines. *Neuron* 2006, *52*, 635-648.
19. Borromeo, M.; Marchesoni, F.; Ghosh, P.K. Communication: Driven Brownian transport in eccentric septate channels. *J. Chem. Phys.* 2011, *134*, 051101.
20. Bernate, J.A.; Drazer, G. Stochastic and deterministic vector chromatography of suspended particles in one-dimensional periodic potentials. *Phys. Rev. Lett.* 2012, *108*, 214501.
21. Bernate, J.A.; Liu, C.; Lagae, L. Konstantopoulos, K.; Drazer, G. Vector separation of particles and cells using an array of slanted open cavities. *Lab Chip* 2013, *13*, 1086.
22. Deng, C.; Luo, M.K.; Xu, L.; Zhao, Q. Transport properties of coupled Brownian particles confined to a microchannel in an asymmetric periodic potential. *Chinese journal of physics* 2019, *62*, 106-114.
23. Bao, F.B.; Hao, H.B.; Yin, Z.q.; Tu, C.X. Numerical study of nanoparticle deposition in a gaseous microchannel under the influence of various forces. *Micromachines* 2021, 12, 47.
24. Milad Ramezanpour, Majid Siavashi, Ali Q. Raeini, Martin J. Blunt. Pore-scale simulation of nanoparticle transport and deposition in a microchannel using a Lagrangian approach. Journal of *Molecular Liquids* 2022 355, 118948.

25. Khatri, Narender.; Burada, P.S. Diffusion of chiral active particles in a Poiseuille flow. *Phys. Rev. E* 2022, *105*, 024604
26. Acharya, A.; Jana, K.; Gurvic, D.; Zachariae, U.; Kleinekathöfer U. Fast prediction of antibiotic permeability through membrane channels using Brownian dynamics. *Biophysical Journal* 2023, 122, 2996–3007.
27. Guo, R.X.; Ai, B.Q. Directed transport of deformable self-propulsion particles in an asymmetric periodic channel. *Acta Phys. Sin.* 2023, *72*, 200501.
28. Almeida1, F.; Gireesha, B.J.; Venkatesh, P.; Nagaraja, B. KKL model for magnetized Al_2O_3-nanoliquid drift in microchannel reckoning Brownian motion. *Int. J. Appl. Comput. Math* 2023, 9, 148.
29. Malgaretti, P.; Nizkaia, T.; Oshanin, G. Splitting probabilities for dynamics in corrugated channels: Passive vs. active Brownian motion. *EPL* 2023, 142, 57001.
30. Bag, P.; Nayak, S.; Ghosh, P.K. Particle–wall alignment interaction and active Brownian diffusion through narrow channels. *Soft Matter* 2024, 20, 8267–8277.
31. Rajkumar, D.; Reddy, A.S.; Govindarajalu. K.; Vajravelu, K.; Thamizharasan, T.; Jagadeshkumar, K. Magnetohydrodynamic micropolar nanofluid flow with pulsation in a vertical permeable channel with Brownian motion, thermophoresis, and thermal radiation: a Buongiorno model approach. *Physica scripta* 2025, *100*, 15205
32. Braun, O.M.; Kivshar, Y.S. *The Frenkel-Kontorova model: Concepts, Methods, and Applications*; Springer: Berlin, Germany, 2004; pp. 2-20.
33. Li, C.P.; Chen, H.B.; Zheng, Z.G. Double-temperature ratchet model and current reversal of coupled Brownian motors. *Front. Phys*. 2017, *6*, 43-52.
34. Kumar, K.V.; Ramaswamy, S.; Rao, M. Active elastic dimers: Self-propulsion and current reversal on a featureless track. *Phys. Rev. E* 2008, *77*, 020102.